

No Attention is Needed: Grouped Spatial-temporal Shift for Simple and Efficient Video Restorers

Dasong Li¹ Xiaoyu Shi¹ Yi Zhang¹ Xiaogang Wang^{1,3} Hongwei Qin² Hongsheng Li^{1,3}

¹ The Chinese University of Hong Kong ² SenseTime Research

³ Centre for Perceptual and Interactive Intelligence Limited

Abstract

Video restoration, aiming at restoring clear frames from degraded videos, has been attracting increasing attention. Video restoration is required to establish the temporal correspondences from multiple misaligned frames. To achieve that end, existing deep methods generally adopt complicated network architectures, such as integrating optical flow, deformable convolution, cross-frame or cross-pixel self-attention layers, resulting in expensive computational cost. We argue that with proper design, temporal information utilization in video restoration can be much more efficient and effective. In this study, we propose a simple, fast yet effective framework for video restoration. The key of our framework is the grouped spatial-temporal shift, which is simple and lightweight, but can implicitly establish inter-frame correspondences and achieve multi-frame aggregation. Coupled with basic 2D U-Nets for frame-wise encoding and decoding, such an efficient spatial-temporal shift module can effectively tackle the challenges in video restoration. Extensive experiments show that our framework surpasses previous state-of-the-art method with 43% of its computational cost on both video deblurring and video denoising.

1 Introduction

With the rapid development of smartphones, capturing videos becomes popular. However, the videos usually suffer from different types of degradations, such as image noise due to low-cost sensors and severe blurs caused by camera shaking and object moving. Video restoration, aiming to recover clear frames from degraded videos, has been attracting increasing attention in recent years. Video restoration, by nature, requires aggregating information from the temporal dimension. Two decisive functionalities and challenges of video restoration are *alignment* and *information aggregation* across frames. The keys of various video restoration network lie in how to design different network components to realize the two functionalities.

For inter-frame alignment, most previous video restoration methods resort to explicit alignment to establish temporal correspondences across frames, such as using optical flow [51] and deformable convolution [10, 56]. However, using such techniques incurs more computational cost and memory consumption. They might also fail in the scenarios of large displacements [25], noise [7, 53], and blurry regions [40, 6]. Several methods [32, 43, 6, 33, 50] utilize convolutional networks to fuse multiple frames without explicit inter-frame alignment, which generally show poorer performances. Information aggregation across frames is mostly dominated by recurrent frameworks. However, the misalignments and faulty prediction can be accumulated across time and the methods are usually difficult to be parallelized for efficient inference. Recently, transformer architectures [11, 14] emerge as promising alternatives. Video restoration transformer (VRT) [27] is proposed for modeling long-range dependency with attention mechanism. Nevertheless, VRT has a very large number of self-attention layers and is computationally costly.

Previous methods tackling the two challenges are either computationally expensive or have complicated network architectures. In this study, we propose a simple, fast, and effective spatial-temporal shift module to implicitly model temporal correspondences across time. We introduce Group Shift-Net, which is equipped with the proposed spatial-temporal shift module for alignment and basic 2D U-Nets as the frame-wise encoder and decoder. Such a simple yet effective framework is able to model long-term dependency without utilizing resource-demanding optical flow estimation [51], deformable convolution [10, 44, 47], recurrent methods [32, 3, 5, 40, 6], or temporal transformers [27]. Our Group Shift-Net adopts a three-stage design: 1) frame-wise pre-restoration, 2) multi-frame fusion with grouped spatial-temporal shift, and 3) frame-wise restoration:

1. **Frame-wise Pre-restoration.** The presence of severe degradation (e.g., noise and blur) would significantly impede the establishment of temporal correspondences between frames. The main goal of the first stage is to mitigate the adverse effect by performing per-frame initial restoration, for which 2D frame-wise U-Nets are adopted.
2. **Multi-frame fusion.** We propose a simple and lightweight grouped spatial-temporal shift module to realize implicit temporal alignment and effective multi-frame feature aggregation. The features of an input clip are separately shifted in spatial and temporal dimensions, and fused by 2D convolution blocks. Such shift operations have minimal computational cost, but can still achieve long-term information aggregation by stacking multiple spatial-temporal shift blocks.
3. **Frame-wise restoration.** After the multi-frame features are implicitly aggregated, 2D frame-wise U-Nets are adopted for reconstructing each frame’s final result.

Notably, our proposed grouped spatial-temporal shift module is quite different from the temporal shift module (TSM) [28] for video understanding. Directly applying TSM cannot achieve promising performance in low-level video restoration. Our method has three key differences with TSM: a) *Channel misalignment in TSM.* TSM [28] adopts bi-directional channel shift during training. The channels of the reference frame and two neighboring frames would misalign and actually increase the difficulty of multi-frame aggregation. Our module advocates alternative temporal shifts to achieve bi-directional communication. b) *No spatial shift in TSM.* In TSM [28], shift is only applied along the channel dimension, which is incapable of conducting alignment. The proposed grouped spatial-temporal shift performs additional spatial shift on the features of neighboring frames. The additional spatial shift, has different directions and strides and thus provides multiple candidate displacements for matching misaligned features. c) *Depth-wise Convolution with Large Kernels.* To further handle the possible large displacements between frames, we adopt depth-wise convolutions with large kernels [30, 13, 15] to increase the receptive field.

The contributions of this study are two-fold: 1) We propose a simple, fast, yet effective framework with a newly introduced grouped spatial-temporal shift, made for video restoration, which achieves efficient temporal feature alignment and aggregation when coupled with only basic 2D convolution blocks. 2) The proposed framework achieves state-of-the-art performances with much fewer FLOPs on both video deblurring and video denoising tasks, demonstrating its generalization capability.

2 Related Work

A series of learning-based methods have been proposed to explore *temporal alignment* and *long-term information aggregation* for video restoration.

Temporal alignment. Temporal alignment is a vital step to model temporal correspondences of misaligned frames in videos. Early learning-based methods [21, 2, 42, 40, 24] employ traditional image alignment methods [48] to model the motions. To handle complicated motions, Xue et al. [51] propose task-oriented flow by fine-tuning a pretrained optical flow model [37] on different video restoration tasks. Dynamic filters [20, 55] and deformable convolution [44, 47] are also proposed to achieve implicit motion compensation. Chan et al. [5, 27] leverage the optical flow to guide the deformable alignment for stable training [4]. Such temporal alignment techniques increase the model complexity and might fail in the case of large displacement [25], noise [7, 53], blurry regions [40, 6]. A series of methods [43, 6, 32] are proposed to avoid explicit motion compensation. Chao et al. [6] demonstrate that optical flow and deformable convolution cannot model the motions or restore sharp frame in video deblurring, due to the blur effect. FastDVDNet [43] and EMVD [32] also propose to

utilize convolution networks to handle motion implicitly. However, convolution usually has narrow receptive field, which limits the model capacity to address large displacements.

Long-term information aggregation. To obtain the long-term information from distant frames, learning-based methods can be mainly divided into two categories: 1) sliding window-based methods and 2) recurrent methods. Sliding window-based methods [43, 36] usually take several adjacent frames as input and output the center restored frame. The information can only be propagated within the fixed sliding window. The sliding window-based methods also suffer from inefficient computation. In contrast, the recurrent methods propagate information recurrently. A series of methods [18, 40, 32, 3, 5] utilize the recurrent framework for long-term information propagation. In recurrent methods, the faulty prediction and misalignment are accumulated frame by frame, which would deteriorate the long-term dependency modeling. Additionally, the recurrent methods are limited in parallelization for efficient inference.

Shift operations. Wu et al. [49] propose to combine shift operation and 1×1 convolution as an efficient alternative to 3×3 convolution. Its variants [19, 9] propose learnable active shifts. Lin et al. [28] propose a temporal shift module (TSM) for video understanding. Based on TSM, Rong et al. [38] apply unidirectional temporal shift on wavelet transforms for burst denoising. Liu et al. [29] propose to perform self-attention calculation with shifted windows to boost the performance of vision transformer [14]. Recently, a series of MLP-based architectures [46, 26, 52] couple the spatial shifts with multi-layer perceptron to achieve the competitive performance in high-level visions tasks. Liang et al. [27] propose a video restoration transformer (VRT), where one video is partitioned into 2-frame clips at each layer and shifted for every other layer to perform temporal self attention. However, it has a large number of self-attention layers and produces a large amount of computational cost.

3 Method

3.1 Overall Pipeline of Group Shift-Net

Most previous methods in video restoration adopt complicated and resource-demanding network architectures, such as optical flow prediction [51], deformable convolution [10], and temporal self-attention layers [27]. We propose a simple yet effective grouped spatial-temporal shift module with 2D basic U-Nets [39] to implicitly establish temporal correspondences. Given consecutive degraded frames $\{I_i \in \mathbb{R}^{H \times W \times C_{in}}\}_i^T$, where T denotes the frame number, the proposed framework Group Shift-Net outputs the corresponding high-quality frames $\{O_i \in \mathbb{R}^{H \times W \times C_{out}}\}_i^T$. As shown in Figure 1, our framework adopts a three-stage design: 1) frame-wise pre-restoration, 2) multi-frame feature fusion with grouped spatial-temporal shift, and 3) frame-wise restoration.

Frame-wise pre-restoration. In video restoration, each frame suffers from degradation (e.g., noise or blur), which would affect the modeling of temporal correspondences across frames. To mitigate the negative impact of degradation, a 2D frame-wise U-Net-like structure [39] is adopted for frame-wise pre-restoration. The ground-truth frames act as supervisions on the outputs and the frame-wise features $\{f_i \in \mathbb{R}^{H \times W \times C}\}_i^T$ are fed into the next stage for inter-frame alignment and fusion.

Multi-frame feature fusion. At this stage, we propose a grouped spatial-temporal shift block to shift different features groups of neighboring frames to the reference frame to establish the temporal correspondences implicitly. The key-frame feature $f_i \in \mathbb{R}^{H \times W \times C}$ is fully aggregated with those of the neighboring frames to obtain the corresponding aggregated feature $A_i \in \mathbb{R}^{H \times W \times C}$. Spatial-temporal shifts of different directions and distances are adopted to provide multiple candidate displacements for matching the frames. By stacking multiple such grouped spatial-temporal shift blocks, our framework can achieve long-term aggregation with lightweight shift operations.

Frame-wise restoration. At the last stage, a U-Net-like structure, similar to that in stage 1, takes the low-quality input frames $\{I_i\}_i^T$ and corresponding aggregated features $\{A_i\}_i^T$ from the previous stage as input and estimates each frame’s final result O_i .

3.2 U-Net for Frame-wise Restoration

For the network of frame-wise pre-restoration of stage 1 and final restoration of stage 3, it is observed in 4c that a single U-Net-like structure [39, 54] cannot restore the frames well. Instead, we propose to stack N 2D slim U-Nets consecutively to conduct frame-wise restoration effectively. Stacking

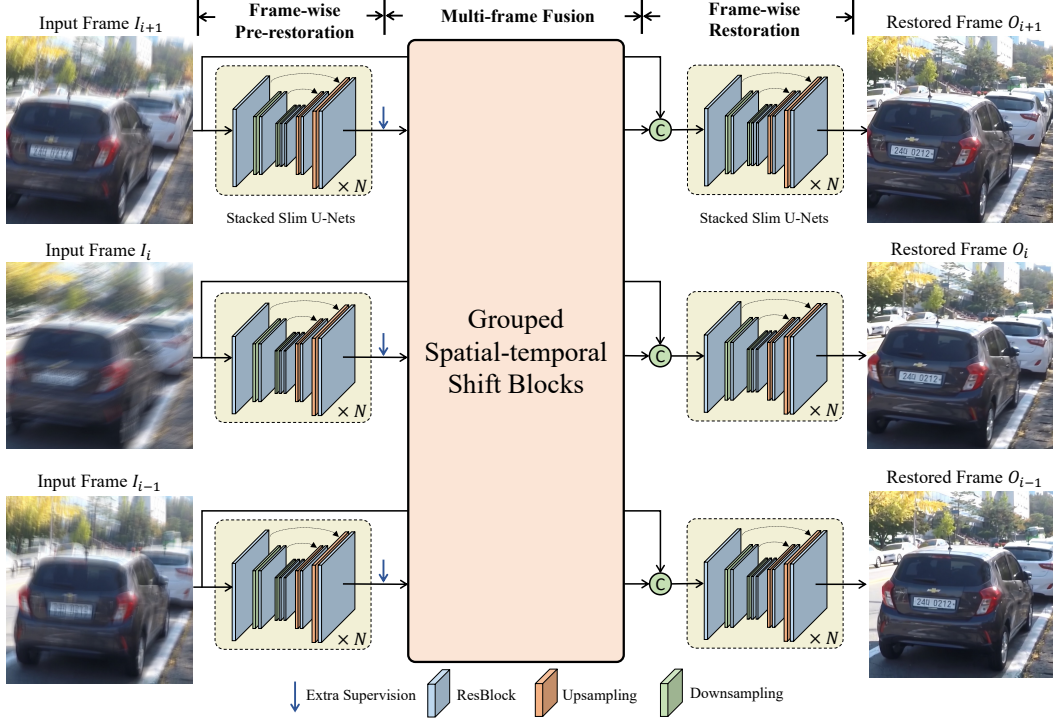


Figure 1: The overview of the Group Shift-Net. It adopts a three-stage design: frame-wise pre-restoration, multi-frame fusion, and final restoration. At the second stage, we utilize grouped spatial-temporal shift blocks to achieve multi-frame aggregation.

multiple U-Nets was explored long before [35], which leads to a deeper network depth and achieves larger receptive field than a single U-Net [54] with the same computational cost. At each U-Net, we utilize residual blocks [16] to enhance features at three scales. We adopt average pooling and bilinear upsampling to adjust the resolution of features. The output features of the previous U-Net are directly passed to the next U-Net as input. No other shortcut or loss function is adopted between two U-Nets. Zamir et al. [54] propose to add a cross U-Net feature fusion between two adjacent U-Nets. But adopting this design between our adjacent slim U-Nets achieves worse performance. The outputs of stage 1 and stage 3 are supervised by the ground-truth clean frames with L_1 loss.

3.3 Grouped Spatial-temporal Shift for Multi-frame Fusion

In multi-frame fusion, each frame-wise feature f_i is to be fully aggregated with neighboring features $\{f_{i-t}, \dots, f_{i+t}\}$ to obtain the temporally aligned and fused features F_i . The input features $f_i \in \mathbb{R}^{H \times W \times C}$ have the same resolution as the original input image I_i . Our multi-frame fusion module adopts a three-scale U-Net [39] like structure. We keep skip connections in the U-Net but replace the conventional 2D convolution blocks by the proposed grouped spatial-temporal shift (GSTS) blocks to aggregate multi-frame features. We utilize 2D average pooling and bilinear upsampling for downsampling and upsampling feature maps in the U-Net, respectively. At each scale, we stack multiple GSTS blocks (e.g., 6) to effectively establish temporal correspondences and conduct multi-frame fusion. A GSTS block consists of three components: 1) a temporal shift operation, 2) a spatial shift operation, and 3) a lightweight fusion layer, organized in the way shown in Figure 2.

Grouped temporal shift. It is observed in 4a that, due to the misalignment between frames, handling information from three frames simultaneously [28] would increase the difficulty of multi-frame fusion. Therefore, we only allow each temporal shift to handle two adjacent frames at a time. Our grouped temporal shift blocks are either a forward temporal shift (FTS) block fusing $\{f_{i-1}, f_i\}$ (see Figure 2 Left) or backward temporal shift (BTS) block fusing $\{f_{i+1}, f_i\}$ (see Figure 2 Right). To achieve effective bi-directional temporal propagation, we stack FTS blocks and BTS blocks alternatively.

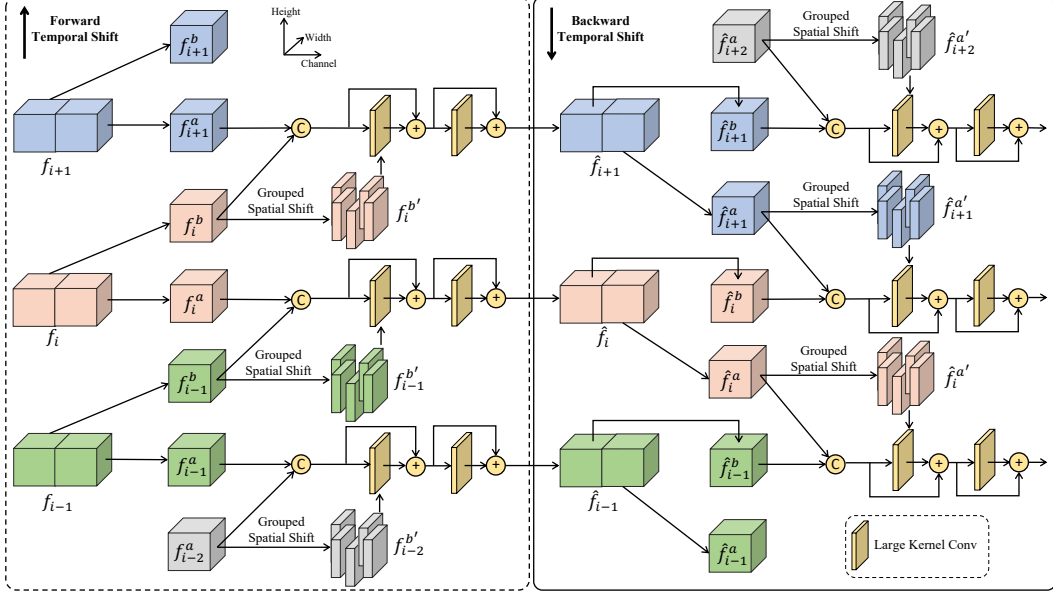


Figure 2: The overview of Grouped Spatial-temporal Shift (GSTS). We stack the forward temporal shift (FTS) blocks (*Left*) and backward temporal shift (BTS) blocks (*Right*) alternatively to achieve bi-directional propagation. In the temporal shift, grouped spatial shift is conducted to provide multiple candidate displacements within a large spatial range and to implicitly establish temporal correspondences. The fusion layer, consisting of two large-kernel convolutions, fuses the multi-frame features after the grouped spatial-temporal shift.

In a temporal shift, the multi-frame features $f_i \in \mathbb{R}^{H \times W \times C}$ are first split (i.e. grouped) equally along the channel dimension to obtain two feature groups: $f_i^a \in \mathbb{R}^{H \times W \times \frac{C}{2}}$ and $f_i^b \in \mathbb{R}^{H \times W \times \frac{C}{2}}$. In the forward shift, f_i^a is not shifted and is aggregated with the forward-shifted feature f_{i-1}^b from time $i - 1$. In the backward shift, f_i^a is backward-shifted to be aggregated with f_{i-1}^b for restoring I_{i-1} . In other words, both FTS and BTS blocks keep half of the feature channels (one feature group) for characterizing visual appearance at current time i and shift the other half of the feature channels (the other feature group) for temporally propagating information for inter-frame aggregation of two frames. For simplicity, in the following paragraphs, we explain the details of the FTS block (i.e. how f_i^a is aggregated with f_{i-1}^b), and the BTS block is similarly defined.

Grouped spatial shift. Directly concatenating f_i^a and f_{i-1}^b for restoring frame i does not account for the spatial misalignment between the two frames i and $i - 1$. Therefore, we propose to conduct additional grouped spatial shift on the propagated feature group $f_{i-1}^b \in \mathbb{R}^{H \times W \times \frac{C}{2}}$ to achieve a large spatial range for the implicit alignment. Specifically, we first equally split (i.e. group) f_{i-1}^b along channel dimension to obtain M feature slices $f_{i-1,m}^b \in \mathbb{R}^{H \times W \times \frac{C}{2M}}$, where $m = 1, \dots, M$ is the slice index. For each feature slice $f_{i-1,m}^b$, we spatially shift it by $(\Delta x_m, \Delta y_m)$ pixels in the x and y directions respectively to obtain the shifted feature slice $f_{i-1,m}^{b'}$.

$$f_{i-1,m}^{b'} = \text{Shift}(f_{i-1,m}^b, \Delta x_m, \Delta y_m), \text{ for } m = 1, \dots, M \quad (1)$$

Since the spatial shift causes void pixels in the border, we set them to zero. To handle objects across two shifts (e.g. Δx_m pixels shift and $2 \times \Delta x_m$ pixels shift), we replace the last pixel shift by a depth-wise 3×3 convolution to achieve smooth translation and combination between two adjacent shifted feature slices. For a Δx_m pixels shift, the corresponding feature group is shifted spatially by $\Delta x_m - 1$ pixels, followed by a depth-wise 3×3 convolution. Then we concatenate all feature groups $f_{i-1,m}^{b'}$ along the channel dimension to obtain the spatially shifted feature $f_{i-1}^{b'}$.

$$f_{i-1}^{b'} = \text{Concat}(f_{i-1,1}^{b'}, \dots, f_{i-1,M}^{b'}). \quad (2)$$

For example, when $M = 9$ and $\Delta x_m, \Delta y_m \in \{-1, 0, 1\}$, the spatial shift operation creates 9 feature slices and shifts the different slices by the 9 directions. In our final implementation, we set $M = 25$

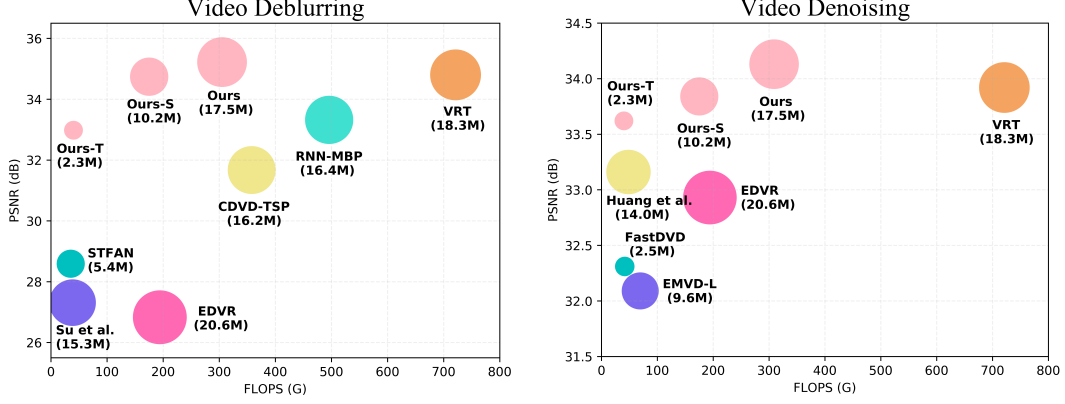


Figure 3: PSNR-Params-FLOPS comparisons with other state-of-the-art methods on video deblurring (Left) and video denoising (Right). The horizontal axis, vertical axis and circle radius represent Flops (computational cost), PSNR (restoration quality) and parameter number (memory overhead), respectively. Our tiny (-T), small (-S) and base models occupy top-left corners, indicating superior performance with higher efficiency.

and $\Delta x_m, \Delta y_m \in \{-10, -5, 0, 5, 10\}$ to enlarge the alignment and fusion’s receptive field, so as to handle large displacements across frames.

Fusion layer. Then we utilize a lightweight fusion layer F with residual connection to aggregate the multi-frame features $f_i^a, f_{i-1}^b, f_{i-1}^{b'}$. The fusion layer F contains two residual blocks and each residual block adopts the combination of point-wise convolution and depth-wise convolution to avoid heavy computation. The output fused feature \hat{f}_i of the reference frame i is calculated as

$$\hat{f}_i = \text{Concat}(f_i^a, f_{i-1}^b) + F(f_i^a, f_{i-1}^b, f_{i-1}^{b'}). \quad (3)$$

The output feature \hat{f}_i of the reference frame i is then fed into the next GSTS block. To further increase the receptive field and to better handle large displacements, we use large-kernel convolutions to handle features from the spatial-temporal shift layer.

4 Experiments

We evaluate Group Shift-Net on two mainstream video restoration tasks: video deblurring and video denoising. To meet different computational requirements, we obtain a series of models of tiny (-T), small (-S) and base size. We also conduct extensive ablation experiments to validate the proposed modules and show impacts of different design choices.

Datasets. For video deblurring, we use GOPRO [34] (CC BY 4.0 license) and DVD [41] datasets. GOPRO [34] dataset contains 2,103 and 1,111 frames as training and test sets, respectively. DVD [41] includes 5,708 frames for training and 1,000 frames for testing. For each dataset, we train our proposed model using its training set and evaluate on the corresponding test set. For video denoising, we follow Huang et al. [17] to train our model on DAVIS [22] dataset and test it on Set8 dataset [43] of different noise levels to test models’ generalization capacity. The Set8 dataset consists of 4 sequences from the *Derfs Test Media collection* and 4 clips captured by a GoPro camera. Our non-blind model is trained for noise level $\sigma \in \mathcal{U}[5, 55]$ during training and tested on different noise levels.

Implementation details. Our Group Shift-Net is end-to-end trained. Separate models are trained for different tasks. The number of channels is 42 for frame-wise restoration and 80 for grouped spatial-temporal shift (GSTS) blocks. In frame-wise pre-restoration and final restoration, 6 slim U-Nets are stacked to encode frame-wise features. In multi-frame fusion, there are 48 GSTS blocks built in a three-scale U-Net-like structure. In the GSTS block, the kernel size of convolution is set to 5×5 . The re-parameterization technique [12] is adopted for better optimization of the large-kernel convolutions. The networks are trained with a batch size of 8 for 750 epochs. The patch size is set as 256×256 . Horizontal and vertical flips are adopted for data augmentation. We use the Adam optimizer [23] and the learning rate is decreased from 3×10^{-4} to 1×10^{-7} according to the cosine annealing strategy [31]. All models are trained on a server with 8 A100 GPUs.

Method	EDVR [47]	Su et al. [41]	STFAN [55]	TSP [36]	MPRNet [54]	HINet [8]	RNN-MBP [6]	VRT [27]	Ours
PSNR	26.83	27.31	28.59	31.67	32.66	32.71	33.32	34.81	35.22
SSIM	0.843	0.826	0.861	0.928	0.959	0.959	0.963	0.972	0.975
Params (M)	20.6	15.3	5.37	16.17	20.1	88.7	16.4	18.3	17.5
FLOPS (G)	194.2	38.7	35.4	357.9	760.1	170.7	496.0	721.3	309.1

Table 1: Quantitative comparison with state-of-the-art video deblurring methods on GoPro [34].

Method	EDVR [47]	Su et al. [41]	STFAN [55]	TSP [36]	PVDNet [40]	ARVo [25]	RNN-MBP [6]	VRT [27]	Ours
PSNR	28.51	30.01	31.15	32.13	32.31	32.80	33.32	34.27	34.52
SSIM	0.864	0.887	0.9049	0.927	0.926	0.9352	0.9627	0.965	0.969

Table 2: Quantitative comparison with state-of-the-art video deblurring methods on DVD [41].

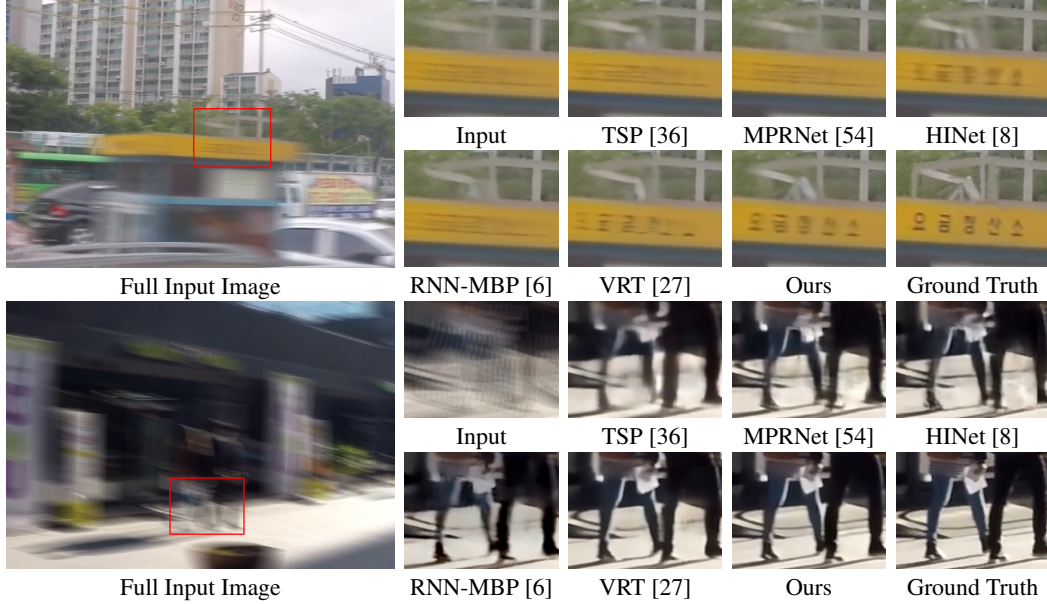


Figure 4: Video deblurring results on hard cases of the GoPro dataset [34]. Our method recovers more details than other methods.

4.1 Video Deblurring Results

Quantitative Comparison. We compare our method with state-of-the-art deblurring methods, EDVR [47], Su et al. [41], STFAN [55], TSP [36], MPRNet [54], HINet [8], RNN-MBP [6], and VRT [27]. As shown in Tables 1 and 2, our model achieves the best restoration quality with high efficiency. Our model outperforms VRT [27], the most competitive method at present, by 0.41 dB and 0.25 dB PSNR on GoPro and DVD, respectively, with only 43% of its flops. For a more intuitive comparison, we provide the PSNR-Params-FLOPS plot in Figure 3 (Left). The three versions of our model occupy the top-left corner, showing strong performance with less computational cost. Notably, our small-version model surpasses EDVR [47] by a significant 7.9 dB PSNR with only 49.5% parameters, our tiny-version model achieves 4.4 dB PSNR gains over STFAN [55] with 42.8% parameters.

Qualitative Comparison. Figure 4 provides the visualization of two hard deblurring cases. As one can see from the full images, there exist severe blurry regions due to camera shaking and object movement. On the zoomed-in patch of the yellow band in the first row, our model reconstructs much sharper letters and building structures. For the walking people in the second row, the fine-grained boundaries of moving legs are better restored by our model.

4.2 Video Denoising Results

Quantitative Comparison. We compare our method with state-of-the-art video denoising methods, VLNB [1], DVDNet [42], FastDVDNet [43], EMVD-L [32], PaCNet [45], EDVR [47], and VRT [27]. In Table 3, we present the quantitative results on Set8 dataset. Our model achieves the best results in 4 out of 5 noise levels. Our method surpasses VRT by 0.55 dB PSNR in the extremely noisy case ($\sigma = 50$). On average, our model achieves 0.21 dB improvement over VRT [27] with 43% FLOPS. Similarly, we provide PSNR-Params-FLOPS in Figure 3 (Right). Our models dominate the top-left

	VLNB [1]	DVDNet [42]	FastDVD [43]	EMVD-L [32]	PaCNet [45]	EDVR [47]	Huang et al. [17]	VRT [27]	Ours
$\sigma = 10$	37.26	36.08	36.44	36.56	37.06	37.16	37.17	37.88	37.54
$\sigma = 20$	33.72	33.49	33.43	33.27	33.94	34.09	34.22	35.02	35.10
$\sigma = 30$	31.74	31.79	31.68	31.40	32.05	32.31	32.57	33.35	33.64
$\sigma = 40$	30.39	30.55	30.46	30.05	30.70	31.03	31.39	32.15	32.60
$\sigma = 50$	29.24	29.56	29.53	29.15	29.66	30.06	30.45	31.22	31.77
Average	32.47	32.29	32.31	32.09	32.68	32.93	33.16	33.92	34.13
Params (M)	-	-	2.5	9.6	2.87	20.6	13.95	18.3	17.5
FLOPS (G)	-	-	41.8	69.5	-	194.2	48.5	721.3	309.1

Table 3: Quantitative comparison with state-of-the-art video denoising methods on Set8 [43].

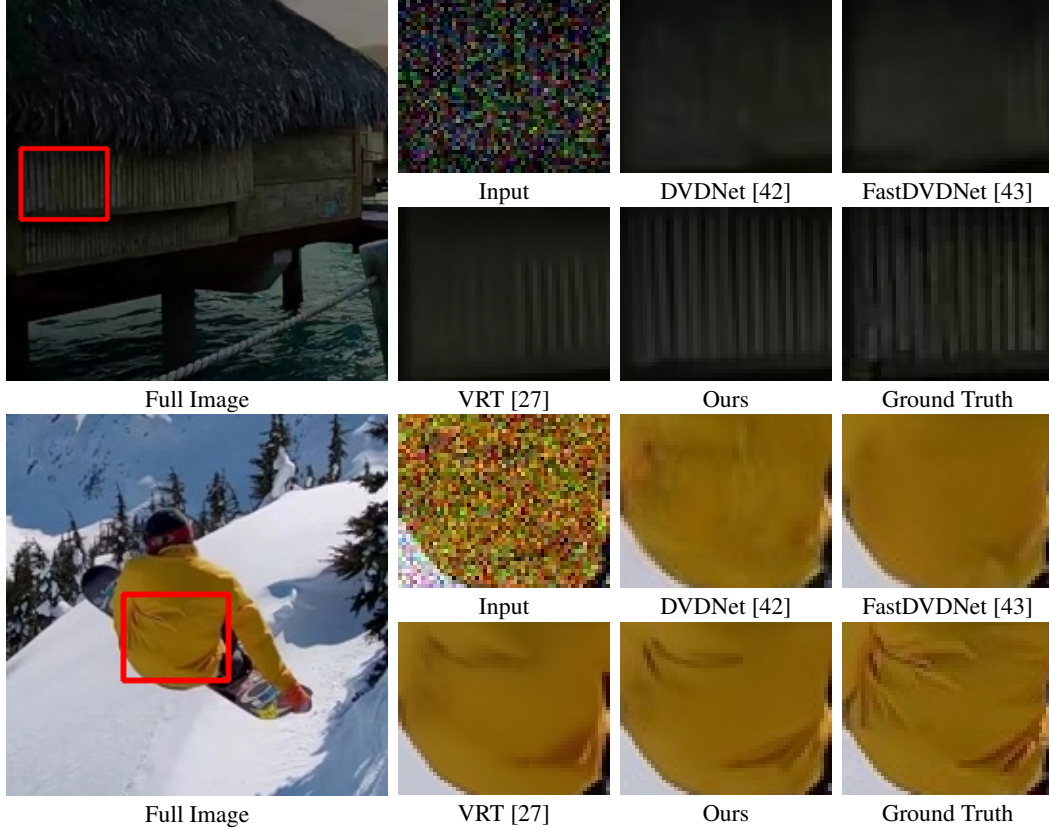


Figure 5: Video denoising results on Set8. Our method achieves better performances at reconstructing details such as textures and lines.

corner, exhibiting superior performance and efficiency advantages. Specifically, our small-version model outperforms EDVR [47] by a clear margin of 0.91 dB with only 49.5% parameters, our tiny-version model leads Huang et al. [17] by 0.46 dB with only 16.5% of its parameters.

Qualitative Comparison. Figure 5 visualizes the denoising results of severe noisy videos of the Set8 [43]. Note the zoomed-in regions in the red boxes. Other models generate over-smooth results, while our model reconstructs more detailed textures, showing the superiority of our models.

4.3 Ablation Study

We demonstrate the effectiveness of each key component in Group Shift-Net. All the methods are trained and evaluated on the GoPro dataset [34] with the same training settings of our base model.

Grouped spatial-temporal shift. To demonstrate the effectiveness of grouped spatial-temporal shift (GSTS) block, we remove *grouped spatial shift* and *alternative temporal shift* gradually to evaluate the impact of each component. The results are shown in Table 4a. At first, We remove *grouped spatial shift* and only the temporal shift is applied. It suffers a drop of 0.33 dB PSNR. Then we replace the alternative temporal shift by the bi-directional shift, where a fusion layer would aggregate $\frac{3}{4}$ channels of feature f_i , $\frac{1}{8}$ channels of feature f_{i-1} , and $\frac{1}{8}$ channels of feature f_{i+1} . This operation causes a decrease of 0.31 dB PSNR. The ablation study of two steps demonstrates the importance of *grouped spatial shift* and *alternative temporal shifts*.

Spatial Shift	Alternative Temporal Shift	Bi-directional Temporal Shift	PSNR
\times	\times	\checkmark	34.58
\times	\checkmark	\times	34.89
\checkmark	\checkmark	\times	35.22

(a) Ablation of grouped spatial-temporal shift.

Pre-restoration	Extra Supervision	PSNR
\times	\times	34.95
\checkmark	\times	34.93
\checkmark	\checkmark	35.22

(b) Ablation of pre-restoration.

N	$N = 1$	$N = 2$	$N = 3$	$N = 4$	$N = 5$	$N = 6$	$N = 7$
PSNR	34.90	34.96	35.06	35.16	35.17	35.22	34.94

(c) Ablation of stacking N slim U-Nets in frame-wise processing.

Kernel	3×3	5×5	7×7	9×9
PSNR	34.93	35.22	35.17	35.13

(d) Ablation of kernel size.

$\Delta x_m, \Delta y_m$	$\{0\}$	$\{0, \pm 1, \pm 2\}$	$\{0, \pm 2, \pm 4\}$	$\{0, \pm 3, \pm 6\}$	$\{0, \pm 4, \pm 8\}$	$\{0, \pm 5, \pm 10\}$	$\{0, \pm 6, \pm 12\}$	$\{0, \pm 7, \pm 14\}$
PSNR	34.89	35.01	35.12	35.09	35.18	35.22	35.20	34.90

(e) Ablation of $\Delta x_m, \Delta y_m$ in grouped spatial shift.

$(\Delta x_m, \Delta y_m), M$	$(\{0\}, 1)$	$(\{0, \pm 5\}, 9)$	$(\{0, \pm 5, \pm 10\}, 25)$	$(\{0, \pm 5, \pm 10, \pm 15\}, 49)$
PSNR	34.89	35.11	35.22	35.21

(f) Ablation of $(\Delta x_m, \Delta y_m), M$ in grouped spatial shift.

Stacking multiple U-Nets. The stacked U-Nets are chosen as the network architecture for frame-wise pre-restoration and final restoration. We start from a single standard U-Net-like structure and gradually increase the number N of the stacked U-Nets. As the stacking number N increases, the channel of U-Net becomes smaller to maintain the equal computational cost. It is observed in Table 4c that the performance of stacking N slim U-Nets gets better as N increases. When $N = 7$, the performance drops significantly. It might be because the channel number of each U-Net becomes too small to encode effective features. The model with 6 slim U-Nets achieves the best performance, which is 0.32 dB PSNR better than using a single U-Net.

Large-kernel convolutions. Then we conduct ablation study of different kernel sizes in multi-frame fusion. $3 \times 3, 5 \times 5, 7 \times 7$ and 9×9 are evaluated to increase the receptive field of the large-kernel convolutions. It is observed in Table 4d that using the kernel size of 5×5 improves over 3×3 ones by 0.29 dB PSNR. However, the performances of 7×7 and 9×9 convolutions drop by 0.05 dB PSNR and 0.09 dB, respectively, which demonstrates that larger kernel sizes cannot improve the performance further. It might be because larger kernels are more difficult to optimize.

Grouped Spatial shift. We set $M = 25$ and change the $\Delta x_m, \Delta y_m$ as shown in Table 4e. $\Delta x_m, \Delta y_m \in \{0\}$ means that only temporal shift is applied. When $\Delta x_m, \Delta y_m \in \{0, \pm 5, \pm 10\}$, the range of spatial shifts is up to 21×21 pixels. It is observed that the model with $\Delta x_m, \Delta y_m \in \{0, \pm 5, \pm 10\}$ achieves the best performance. Then We change the number M of shifts and $\Delta x_m, \Delta y_m$ are changed with the number M . $M = 0$ denotes that no spatial shift is adopted. It is shown in Table 4f that the models with $M = 49$ and $M = 25$ achieve the similar performances, which outperform the model with $M = 9$ by ~ 0.11 dB PSNR. Therefore, we select $M = 25$ and $\Delta x_m, \Delta y_m \in \{0, \pm 5, \pm 10\}$ in our solution.

Frame-wise pre-restoration. We evaluate the impact of frame-wise pre-restoration in Table 4b. First, we remove the extra supervision applied to the output of stage 1. It suffers a drop of 0.29 dB PSNR. Then we move the network of the first stage to the third stage and adopt 12 stacked U-Nets for the third stage. Then the multi-frame fusion of stage 2 would handle the severe degraded frames directly. It also suffers a drop of 0.27 PSNR. The two framework achieve almost the same performances, which are much lower than our final solution. The two experiments demonstrate the importance of extra supervision in frame-wise pre-restoration.

5 Limitation and Conclusion

In this paper, we propose a simple, fast and effective Group Shift-Net for video restoration. Our method does not require complicated network architectures, such as using optical flow, deformable convolution or self-attention layers. In contrast, we propose a grouped spatial-temporal shift block to perform grouped large spatial shifts on multi-frame features to achieve temporal alignment implicitly. With the basic 2D U-Nets, such an efficient block can still establish temporal correspondence and long-term information aggregation. Extensive experiments on various datasets show that our method surpasses the state-of-the-art methods with much less computational cost on video restoration. The

current spatial-temporal shift layers are implemented via PyTorch. Although it has theoretically minimal FLOPs, the implementation of PyTorch is to shift the feature groups one by one, which is not efficient. We will write customized CUDA kernel functions to speed up the spatial-temporal shift layers in the near future. We do not foresee negative social impact from the proposed work.

References

- [1] Pablo Arias and Jean-Michel Morel. Video denoising via empirical bayesian estimation of space-time patches. *J. Math. Imaging Vis.*, 60(1):70–93, jan 2018.
- [2] J. Caballero, C. Ledig, A. Aitken, A. Acosta, J. Totz, Z. Wang, and W. Shi. Real-time video super-resolution with spatio-temporal networks and motion compensation. In *2017 IEEE Conference on Computer Vision and Pattern Recognition (CVPR)*, pages 2848–2857, Los Alamitos, CA, USA, jul 2017. IEEE Computer Society.
- [3] Kelvin CK Chan, Xintao Wang, Ke Yu, Chao Dong, and Chen Change Loy. Basicvsr: The search for essential components in video super-resolution and beyond. In *Proceedings of the IEEE conference on computer vision and pattern recognition*, 2021.
- [4] Kelvin CK Chan, Xintao Wang, Ke Yu, Chao Dong, and Chen Change Loy. Understanding deformable alignment in video super-resolution. In *AAAI Conference on Artificial Intelligence*, 2021.
- [5] Kelvin C.K. Chan, Shangchen Zhou, Xiangyu Xu, and Chen Change Loy. Basicvsr++: Improving video super-resolution with enhanced propagation and alignment. In *arXiv preprint arXiv:2104.13371*, 2021.
- [6] Zhu Chao, Dong Hang, Pan Jinshan, Liang Boyang, Huang Yuhao, Fu Lean, and Wang Fei. Deep recurrent neural network with multi-scale bi-directional propagation for video deblurring. In *AAAI*, 2022.
- [7] Chen Chen, Qifeng Chen, Minh N. Do, and Vladlen Koltun. Seeing motion in the dark. In *Proceedings of the IEEE/CVF International Conference on Computer Vision (ICCV)*, October 2019.
- [8] Liangyu Chen, Xin Lu, Jie Zhang, Xiaojie Chu, and Chengpeng Chen. Hinet: Half instance normalization network for image restoration. In *Proceedings of the IEEE/CVF Conference on Computer Vision and Pattern Recognition (CVPR) Workshops*, pages 182–192, June 2021.
- [9] W. Chen, D. Xie, Y. Zhang, and S. Pu. All you need is a few shifts: Designing efficient convolutional neural networks for image classification. In *2019 IEEE/CVF Conference on Computer Vision and Pattern Recognition (CVPR)*, pages 7234–7243, Los Alamitos, CA, USA, jun 2019. IEEE Computer Society.
- [10] Jifeng Dai, Haozhi Qi, Yuwen Xiong, Yi Li, Guodong Zhang, Han Hu, and Yichen Wei. Deformable convolutional networks. In *Proceedings of the IEEE international conference on computer vision*, 2017.
- [11] Jacob Devlin, Ming-Wei Chang, Kenton Lee, and Kristina Toutanova. Bert: Pre-training of deep bidirectional transformers for language understanding. *arXiv preprint arXiv:1810.04805*, 2018.
- [12] Xiaohan Ding, Xiangyu Zhang, Ningning Ma, Jungong Han, Guiguang Ding, and Jian Sun. Repvgg: Making vgg-style convnets great again. In *Proceedings of the IEEE/CVF Conference on Computer Vision and Pattern Recognition*, pages 13733–13742, 2021.
- [13] Xiaohan Ding, Xiangyu Zhang, Yizhuang Zhou, Jungong Han, Guiguang Ding, and Jian Sun. Scaling up your kernels to 31x31: Revisiting large kernel design in cnns. *arXiv preprint arXiv:2203.06717*, 2022.
- [14] Alexey Dosovitskiy, Lucas Beyer, Alexander Kolesnikov, Dirk Weissenborn, Xiaohua Zhai, Thomas Unterthiner, Mostafa Dehghani, Matthias Minderer, Georg Heigold, Sylvain Gelly, Jakob Uszkoreit, and Neil Houlsby. An image is worth 16x16 words: Transformers for image recognition at scale. In *International Conference on Learning Representations*, 2021.
- [15] Meng-Hao Guo, Cheng-Ze Lu, Zheng-Ning Liu, Ming-Ming Cheng, and Shi-Min Hu. Visual attention network. *arXiv preprint arXiv:2202.09741*, 2022.

- [16] Kaiming He, Xiangyu Zhang, Shaoqing Ren, and Jian Sun. Deep residual learning for image recognition. In *The IEEE Conference on Computer Vision and Pattern Recognition (CVPR)*, June 2016.
- [17] Cong Huang, Jiahao Li, Bin Li, Dong Liu, and Yan Lu. Neural compression-based feature learning for video restoration, 2022.
- [18] Takashi Isobe, Xu Jia, Shuhang Gu, Songjiang Li, Shengjin Wang, and Qi Tian. Video super-resolution with recurrent structure-detail network. *CoRR*, abs/2008.00455, 2020.
- [19] Yunho Jeon and Junmo Kim. Constructing fast network through deconstruction of convolution. In *Proceedings of the 32nd International Conference on Neural Information Processing Systems, NIPS’18*, page 5955–5965, Red Hook, NY, USA, 2018. Curran Associates Inc.
- [20] Younghyun Jo, Seoung Wug Oh, Jaeyeon Kang, and Seon Joo Kim. Deep video super-resolution network using dynamic upsampling filters without explicit motion compensation. In *2018 IEEE/CVF Conference on Computer Vision and Pattern Recognition*, pages 3224–3232, 2018.
- [21] Armin Kappeler, Seunghwan Yoo, Qiqin Dai, and Aggelos K. Katsaggelos. Video super-resolution with convolutional neural networks. *IEEE Transactions on Computational Imaging*, 2(2):109–122, 2016.
- [22] Anna Khoreva, Anna Rohrbach, and Bernt Schiele. Video object segmentation with language referring expressions. In *Asian Conference on Computer Vision*, pages 123–141. Springer, 2018.
- [23] Diederik P. Kingma and Jimmy Ba. Adam: A method for stochastic optimization. In Yoshua Bengio and Yann LeCun, editors, *3rd International Conference on Learning Representations, ICLR 2015, San Diego, CA, USA, May 7-9, 2015, Conference Track Proceedings*, 2015.
- [24] Dasong Li, Yi Zhang, Ka Lung Law, Xiaogang Wang, Hongwei Qin, and Hongsheng Li. Efficient burst raw denoising with variance stabilization and multi-frequency denoising network, 2022.
- [25] Dongxu Li, Chenchen Xu, Kaihao Zhang, Xin Yu 0002, Yiran Zhong, Wenqi Ren, Hanna Suominen, and Hongdong Li. Arvo: Learning all-range volumetric correspondence for video deblurring. In *IEEE Conference on Computer Vision and Pattern Recognition, CVPR 2021, virtual, June 19-25, 2021*, pages 7721–7731. Computer Vision Foundation / IEEE, 2021.
- [26] Dongze Lian, Zehao Yu, Xing Sun, and Shenghua Gao. As-mlp: An axial shifted mlp architecture for vision, 2021.
- [27] Jingyun Liang, Jiezhong Cao, Yuchen Fan, Kai Zhang, Rakesh Ranjan, Yawei Li, Radu Timofte, and Luc Van Gool. Vrt: A video restoration transformer. *arXiv preprint arXiv:2201.12288*, 2022.
- [28] Ji Lin, Chuang Gan, and Song Han. Tsm: Temporal shift module for efficient video understanding. In *Proceedings of the IEEE International Conference on Computer Vision*, 2019.
- [29] Ze Liu, Yutong Lin, Yue Cao, Han Hu, Yixuan Wei, Zheng Zhang, Stephen Lin, and Baining Guo. Swin transformer: Hierarchical vision transformer using shifted windows. In *Proceedings of the IEEE/CVF International Conference on Computer Vision (ICCV)*, 2021.
- [30] Zhuang Liu, Hanzi Mao, Chao-Yuan Wu, Christoph Feichtenhofer, Trevor Darrell, and Saining Xie. A convnet for the 2020s. *CoRR*, abs/2201.03545, 2022.
- [31] Ilya Loshchilov and Frank Hutter. SGDR: stochastic gradient descent with warm restarts. In *5th International Conference on Learning Representations, ICLR 2017, Toulon, France, April 24-26, 2017, Conference Track Proceedings*. OpenReview.net, 2017.
- [32] M. Maggioni, Y. Huang, C. Li, S. Xiao, Z. Fu, and F. Song. Efficient multi-stage video denoising with recurrent spatio-temporal fusion. In *2021 IEEE/CVF Conference on Computer Vision and Pattern Recognition (CVPR)*, 2021.
- [33] Ben Mildenhall, Jonathan T. Barron, Jiawen Chen, Dillon Sharlet, Ren Ng, and Robert Carroll. Burst denoising with kernel prediction networks. In *CVPR*, 2018.
- [34] Seungjun Nah, Tae Hyun Kim, and Kyoung Mu Lee. Deep multi-scale convolutional neural network for dynamic scene deblurring. In *The IEEE Conference on Computer Vision and Pattern Recognition (CVPR)*, July 2017.

- [35] Alejandro Newell, Kaiyu Yang, and Jia Deng. Stacked hourglass networks for human pose estimation. In Bastian Leibe, Jiri Matas, Nicu Sebe, and Max Welling, editors, *Computer Vision – ECCV 2016*, pages 483–499, Cham, 2016. Springer International Publishing.
- [36] Jinshan Pan, Haoran Bai, and Jinhui Tang. Cascaded deep video deblurring using temporal sharpness prior. In *IEEE/CVF Conference on Computer Vision and Pattern Recognition (CVPR)*, June 2020.
- [37] Anurag Ranjan and Michael J. Black. Optical flow estimation using a spatial pyramid network. In *2017 IEEE Conference on Computer Vision and Pattern Recognition (CVPR)*, pages 2720–2729, 2017.
- [38] Xuejian Rong, Denis Demandolx, Kevin Matzen, Priyam Chatterjee, and Yingli Tian. Burst denoising via temporally shifted wavelet transforms. In *Computer Vision – ECCV 2020: 16th European Conference, Glasgow, UK, August 23–28, 2020, Proceedings, Part XIII*, page 240–256, Berlin, Heidelberg, 2020. Springer-Verlag.
- [39] Olaf Ronneberger, Philipp Fischer, and Thomas Brox. U-net: Convolutional networks for biomedical image segmentation. In Nassir Navab, Joachim Hornegger, William M. Wells, and Alejandro F. Frangi, editors, *Medical Image Computing and Computer-Assisted Intervention – MICCAI 2015*, 2015.
- [40] Hyeonseok Son, Junyong Lee, Jonghyeop Lee, Sunghyun Cho, and Seungyong Lee. Recurrent video deblurring with blur-invariant motion estimation and pixel volumes. *ACM Transactions on Graphics (TOG)*, 40(5), 2021.
- [41] Shuochen Su, Mauricio Delbracio, Jue Wang, Guillermo Sapiro, Wolfgang Heidrich, and Oliver Wang. Deep video deblurring for hand-held cameras. In *2017 IEEE Conference on Computer Vision and Pattern Recognition (CVPR)*, pages 237–246, 2017.
- [42] Matias Tassano, Julie Delon, and Thomas Veit. DVDNET: A FAST NETWORK FOR DEEP VIDEO DENOISING. In *2019 IEEE International Conference on Image Processing*, Taipei, Taiwan, September 2019.
- [43] Matias Tassano, Julie Delon, and Thomas Veit. Fastdvdnet: Towards real-time deep video denoising without flow estimation. In *Proceedings of the IEEE/CVF Conference on Computer Vision and Pattern Recognition (CVPR)*, June 2020.
- [44] Yapeng Tian, Yulun Zhang, Yun Fu, and Chenliang Xu. Tdan: Temporally-deformable alignment network for video super-resolution. In *The IEEE Conference on Computer Vision and Pattern Recognition (CVPR)*, June 2020.
- [45] G. Vaksman, M. Elad, and P. Milanfar. Patch craft: Video denoising by deep modeling and patch matching. In *2021 IEEE/CVF International Conference on Computer Vision (ICCV)*, pages 2137–2146, Los Alamitos, CA, USA, oct 2021. IEEE Computer Society.
- [46] Guangting Wang, Yucheng Zhao, Chuanxin Tang, Chong Luo, and Wenjun Zeng. When shift operation meets vision transformer: An extremely simple alternative to attention mechanism, 2022.
- [47] Xintao Wang, Kelvin C.K. Chan, Ke Yu, Chao Dong, and Chen Change Loy. Edvr: Video restoration with enhanced deformable convolutional networks. In *The IEEE Conference on Computer Vision and Pattern Recognition (CVPR) Workshops*, June 2019.
- [48] Philippe Weinzaepfel, Jerome Revaud, Zaid Harchaoui, and Cordelia Schmid. Deepflow: Large displacement optical flow with deep matching. In *2013 IEEE International Conference on Computer Vision*, pages 1385–1392, 2013.
- [49] B. Wu, A. Wan, X. Yue, P. Jin, S. Zhao, N. Golmant, A. Gholaminejad, J. Gonzalez, and K. Keutzer. Shift: A zero flop, zero parameter alternative to spatial convolutions. In *2018 IEEE/CVF Conference on Computer Vision and Pattern Recognition (CVPR)*, pages 9127–9135, Los Alamitos, CA, USA, jun 2018. IEEE Computer Society.
- [50] Z. Xia, F. Perazzi, M. Gharbi, K. Sunkavalli, and A. Chakrabarti. Basis prediction networks for effective burst denoising with large kernels. In *2020 IEEE/CVF Conference on Computer Vision and Pattern Recognition (CVPR)*, 2020.
- [51] Tianfan Xue, Baian Chen, Jiajun Wu, Donglai Wei, and William T Freeman. Video enhancement with task-oriented flow. *International Journal of Computer Vision (IJCV)*, 127(8):1106–1125, 2019.

- [52] T. Yu, X. Li, Y. Cai, M. Sun, and P. Li. S2-mlp: Spatial-shift mlp architecture for vision. In *2022 IEEE/CVF Winter Conference on Applications of Computer Vision (WACV)*, pages 3615–3624, Los Alamitos, CA, USA, jan 2022. IEEE Computer Society.
- [53] Huanjing Yue, Cong Cao, Lei Liao, Ronghe Chu, and Jingyu Yang. Supervised raw video denoising with a benchmark dataset on dynamic scenes. In *IEEE Conference on Computer Vision and Pattern Recognition*, 2020.
- [54] Syed Waqas Zamir, Aditya Arora, Salman Khan, Munawar Hayat, Fahad Shahbaz Khan, Ming-Hsuan Yang, and Ling Shao. Multi-stage progressive image restoration. In *CVPR*, 2021.
- [55] Shangchen Zhou, Jiawei Zhang, Jinshan Pan, Haozhe Xie, Wangmeng Zuo, and Jimmy Ren. Spatio-temporal filter adaptive network for video deblurring. In *Proceedings of the IEEE International Conference on Computer Vision*, 2019.
- [56] Xizhou Zhu, Han Hu, Stephen Lin, and Jifeng Dai. Deformable convnets v2: More deformable, better results. In *Proceedings of the IEEE/CVF Conference on Computer Vision and Pattern Recognition*, pages 9308–9316, 2019.